RSC Advances

PAPER

View Article Online
View Journal | View Issue



Cite this: *RSC Adv.*, 2024, **14**, 28693

# Synthesis, kinetics, mechanisms, and bioactivity evaluations of a novel Zn(II) complex

Anwesha Dey,†[a] Ramesh Kumar, †[b] Bhramar Dutta, [c] Rajib Bandopadhyay,[c] Sankha Chakrabortty, [d] Moonis Ali Khan, [e] Rijuta Ganesh Saratale,[f] Ganesh Dattatraya Saratale,[g] Byong Hun Jeon *[b] and Alak K. Ghosh *[a]

Received 7th May 2024
Accepted 30th August 2024

DOI: 10.1039/d4ra03356f

rsc.li/rsc-advances

Zn(II)-based anticancer drugs can be suitable alternatives to conventional Pt(II)-based drugs because of the unique chemical properties of Zn(II) and low toxicity. In this study, a new hexadentate and heteroleptic Zn(II) complex ($[Zn(bpy)_2(OAc)_2]$, **1**) was prepared with a conventional *N*,*N*-donor ligand (2,2′-bipyridine) and a leaving group (OAc) and characterized *via* ESI-MS, UV-Vis, and FT-IR spectroscopy. Kinetic and mechanistic investigations of **1** were performed using two biologically relevant ligands (DL-penicillamine and L-cysteine) to understand its selectivity and reactivity. Substitution reactions were determined to be two-step processes in the associative activation mode. Bioactivity studies of **1** revealed moderate to strong DNA-binding, cleaving ability, and antimicrobial properties.



## Introduction

Transition metal complexes are being explored as alternative antitumor agents to Pt(II) complexes, owing to their lower toxicity and higher efficacy compared to that of the latter.[1] In particular, Ru(III), Ga, and As complexes have emerged as promising anticancer drugs.[2] Some Zn(II) coordination complexes also showed promising DNA binding ability and antitumor activity.[3,4] This is attributed to their unique chemical properties, diverse biological functionality, and lower toxicity at even higher doses compared to other metals,[5,6] negligible side effects compared to the available anticancer drugs,[7] and affordability.

Zn has three unique chemical properties: (i) it has a $3d^{10}$ electronic configuration in the +2 state; thus, the Zn(II) coordination complexes have no ligand-field stabilization energy.[8] Hence, they do not have preferential geometry and can form readily exchangeable, flexible, but strong complexes with organic ligands;[9] (ii) Zn(II) has a filled 3d orbital and is thus redox inactive. Hence, they are highly stable in biological reactions and can easily enter biological systems without causing oxidative stress-mediated damage; and (iii) Zn(II) is classified as a borderline metal ion by Pearson in 1963.[10] Therefore, it does not have preference among N, O, or S for coordination. In addition, Zn is an essential trace element and the second-most abundant element in the body.[11] It is crucial for all forms of life on the planet. Zn is present in all body fluids and tissues, with maximum fractions in the muscle tissue, skeleton, and liver.[12] It has diverse biological functions owing to its redox-inactive nature. Zn(II) complexes strengthen the immune system;[13] regulate RNA transcription and DNA synthesis;[14] heal wounds;[15,16] maintain cell growth, cell division, differentiation, proliferation,[17] and prostaglandin function;[14] regulate body fluid pH; enhance collagen formation in hair, nails, and skin;[18] and improve memory and mental health.

The physicochemical properties of Zn(II), such as its diamagnetism, strong Lewis acidity, and $d^{10}$ configuration, enable the formation of different coordination geometries with chelating ligands of diverse donor atoms and hapticity.[3] Moreover, Zn(II) complexes have exhibited antiproliferative activity, fast ligand exchange, Lewis acid activation, and catalytic activities in hydrolysis and DNA cleavage.[19,20] In addition, they are non-toxic, even at high dosages. They have a preventative effect on infectious diseases and are less harmful anticancer drugs.[21] In particular, zinc phthalocyanines serve as photosensitizers or light-sensitive compounds during the photodynamic treatment of tumor cells by producing reactive oxygen species (ROS).[22] Moreover, Zn(II) forms dimeric and polymeric complexes with various donor atoms, such as N, O, and S, in ligands of different

[a]*Department of Chemistry, The University of Burdwan, Burdwan (E) 713104, West Bengal, India. E-mail: akghosh@chem.buruniv.ac.in*

[b]*Department of Earth Resources & Environmental, Engineering, Hanyang University, 222-Wangsimni-ro, Seongdong-gu, Seoul 04763, Republic of Korea. E-mail: bhjeon@hanyang.ac.kr*

[c]*Department of Botany, The University of Burdwan, Burdwan (E) 713104, West Bengal, India*

[d]*School of Chemical Engineering, Kalinga Institute of Industrial Technology, Bhubaneswar 751024, Odisha, India*

[e]*Chemistry Department, College of Science, King Saud University, Riyadh 11451, Saudi Arabia*

[f]*Research Institute of Integrative Life Sciences, Dongguk University-Seoul, Ilsandong-gu, Goyang-si, Gyeonggido 10326, Republic of Korea*

[g]*Department of Food Science and Biotechnology, Dongguk University-Seoul, 32 Dongguk-ro, Ilsandong-gu, Goyang-si, 10326, Gyeonggi-do, Republic of Korea*

† These authors contributed equally.

capacities, resulting in complexes of different geometries and coordination. In particular, Zn(II) complexes with N-donor ligands have been extensively explored as anticancer agents.[3]

To further explore the anticancer activity of Zn(II) complexes with N-donor ligands, in this study, we synthesized a six-coordinated Zn(II) complex bearing two N-donor ligands (2,2′-bipyridine; bpy) and two acetate groups and explored its kinetics and anticancer mechanistic aspects. The DNA binding ability, cleaving capacity, and germicidal activity of the Zn(II) complex were evaluated *via* several bioassays. The aromatic ligand bpy serves as a spectator ligand and facilitates a similar donor environment to that of *cis*-diamminedichloroplatinum(II).[23]

# Materials and methods

## Chemicals

All chemicals were reagent-grade and used without further purification. Chemicals, such as $Zn(OAc)_2$, DL-penicillamine, L-cysteine, Tris buffer, pBR322, EtBr, and bpy were purchased from Sisco Research Laboratories Pvt. Ltd (India). Calf thymus DNA (ctDNA) and $AgClO_4$ were purchased from Sigma-Aldrich (USA). Ampicillin and potato-dextrose agar were purchased from Hi-Media (USA). A constant ionic strength was maintained using a $NaClO_4$ (0.1 M) solution, and the pH of all the solutions used for the kinetics experiments was adjusted using 1 M $NaOH/HClO_4$ prior to the experiments.

## Analytical determination

A Shimadzu UV-vis spectrophotometer (Model UV-3600, Japan) was used for spectroscopic scanning. A Hi-Tech stopped-flow spectrophotometer (Model-TB 85) was used to obtain kinetic data at a controlled temperature. A Shimadzu IR Prestige-21 spectrophotometer (Japan) was used to collect FT-IR data. Mass spectra were obtained using ESI-MS equipment (Waters, Model-Xevo G2-XS QTof, USA) in a positive ion mode. A fluorometer (PerkinElmer, Model-L555 USA) was used to monitor fluorescence quenching. Plasmid DNA (pBR322) treated with $[Zn(bpy)_2(OAc)_2]$ (**1**) was analyzed by agarose gel electrophoresis (Bio-Rad, USA).

## Synthesis of 1

Complex **1** was prepared by mixing the aqueous solutions of $Zn(OAc)_2$ and bpy in a 1 : 2 molar ratio. Aqueous solutions were prepared using double-distilled water. The solution of bpy was added to the solution of $Zn(OAc)_2$ dropwise with continuous stirring using a magnetic stirrer for 8 h at 27 °C. The precipitated white solid was filtered and washed three times with distilled water.

## Kinetics evaluation

The reactions of **1** with DL-penicillamine ($L^1$) and L-cysteine ($L^2$) followed pseudo-first-order kinetics at three different concentrations of ligands and four different temperatures at a physiological pH of 7.4. As the reaction progressed, the maximum difference in the absorbances of **1** and the substituted products **2** (product of $L^1$ and **1**) and **3** (product of $L^2$ and **1**) were observed at 300 nm (Fig. 1).

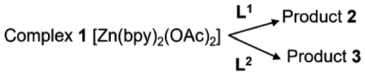


Hence, we monitored the reaction kinetics at 300 nm using five different concentrations ($2.0–4.0 \times 10^3$ mol $L^{-1}$) of $L^1$ and $L^2$ and four different temperatures (20–35 °C).

## Job's method

To determine the effect of continuous variation in the metal: ligand ratio in **2** and **3** and to obtain a bell-shaped curve, we used Job's method.[24,25] Complex **1** and the ligands ($L^1$ and $L^2$) were mixed in an equimolar ratio of $2.0 \times 10^{-4}$ mol $L^{-1}$, and the pH of the solution was maintained at 7.4 at room temperature. The vessel was fitted with a reflux condenser to prevent solvent loss due to evaporation while heating the reaction mixture in a 60 °C water bath.

## Bioassays

**Reaction of 1 with ctDNA.** The electronic absorption titration of **1** with ctDNA was conducted in Tris–HCl buffer (pH 7.4); a fixed concentration (0.1 mM) of **1** was titrated against 0–20 μM ctDNA.[26] The absorption spectra were recorded every 5 min. The binding constant ($K_b$) was determined using the following equation:[27,28]

$$\frac{[DNA]}{(\varepsilon_a - \varepsilon_f)} = \frac{[DNA]}{(\varepsilon_a - \varepsilon_f)} + \frac{1}{K_b(\varepsilon_b - \varepsilon_f)} \quad (1)$$

where $\varepsilon_a$, $\varepsilon_f$, and $\varepsilon_b$ are the extinction coefficients of $A_{obsd}/[\mathbf{1}]$, free **1**, and the fully bonded complex of **1** with ctDNA, respectively. The slope to the intercept ($K_b$) was calculated using the $[DNA]/(\varepsilon_b - \varepsilon_f)$ *vs.* [DNA] plot.[29]

**Fluorescence quenching experiment.** EtBr is a fluorescence tag that exhibits intense fluorescence upon intercalation with

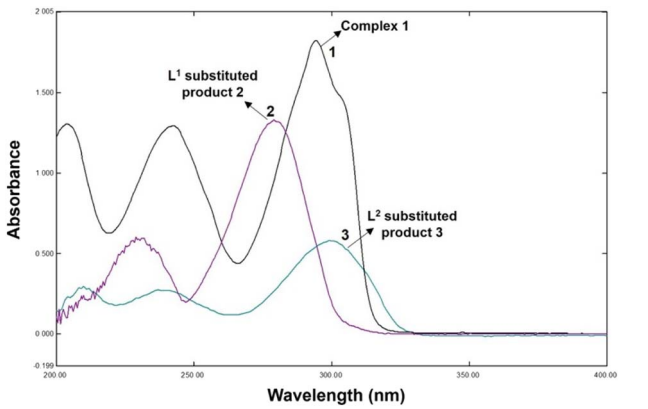


Fig. 1 UV-Vis spectra of $[Zn(bpy)_2(OAc)_2]$ (**1**), DL-penicillamine ($L^1$)-substituted product (**2**), and L-cysteine ($L^2$)-substituted product (**3**). The concentrations of **1** and ligands were $2.0 \times 10^{-4}$ and $4.0 \times 10^{-3}$ mol $L^{-1}$, respectively, and the path length of the quartz cell was 1 cm.

adjacent base pairs of ctDNA. Hence, it was used to evaluate the binding of **1** and ctDNA.[26] The concentration of **1** was increased from 0 to 100 μM in Tris–HCl buffer (pH 7.4) at fixed EtBr and ctDNA concentrations (17 μM). Next, the fluorescence intensities of different solutions were measured at varying ctDNA concentrations. The emission spectra (420–490 nm) of **1**, EtBr, and the DNA solution were measured to determine the quenching constant ($K_{sv}$) at an excitation wavelength of 375 nm. The $K_{sv}$ value was determined using the Stern–Volmer equation as follows:

$$\frac{I_0}{I} = 1 + K_{sv}[Q] \quad (2)$$

where $I_0$ and $I$ are the fluorescence intensities of EtBr–DNA and EtBr–DNA–**1**, respectively, and [Q] is the quencher (**1**) concentration.[30] Furthermore, $K_{app}$, $K_F$, and $n$ are the apparent binding constant, fluorescence binding constant, and total number of binding sites per nucleotide, respectively, which were calculated using eqn (3) and (4).[28]

$$K_{EtBr}[EtBr] = K_{app}[Q] \quad (3)$$

$$\log(F_0 - F)/F = \log K_F + n \log[Q] \quad (4)$$

where [Q] is the quencher concentration at half the fluorescence intensity of EtBr–DNA, $K_{EtBr} = 1.0 \times 10^7\ M^{-1}$, and [EtBr] = 10 μM.

**Plasmid DNA cleavage using 1.** Gel electrophoresis was used to monitor plasmid DNA (pBR 322) cleavage by **1**. Briefly, an aliquot of 150 ng of plasmid DNA solution in 40 mM Tris-acetate buffer (pH 7.2) was reacted with different concentrations of **1**. The final reaction volume was 20 μL. The reaction solution was incubated at 37 °C for 1 h. The sample loading buffer, comprising 0.05% bromophenol blue, 5% glycerol, and 5 μL of 2 mM $H_4$ETDA solution (pH 8.0), the sample (DNA + **1**), and 5 μL EtBr were added to 0.8% agarose gel. Agarose gel electrophoresis was performed at ambient temperature and a voltage of 50 mV for 4 h in the dark.[31]

**Antimicrobial assay.** The disk diffusion method was employed to investigate the *in vitro* antimicrobial activities of the ligand (bpy) and **1**.[32] The *in vitro* antimicrobial activities of **1** were tested against the fungus *Aspergillus niger* (MCC1819); Gram-negative bacteria *Enterobacter asburiae* (GenBank ID MN081607.1) and *Escherichia coli* (NCIM 1056); and Gram-positive bacteria *Staphylococcus aureus* (ATCC 29213), *Bacillus siamensis* (GenBank ID MN134497), *Salinicoccus roseus* (GenBank ID MN080417), and *Halomonas denitrificans* (GenBank ID MN080415).[33,34] Briefly, 100 μL of $10^6$ conidia per mL suspension culture of *Aspergillus niger* was spread over potato dextrose agar plates. In addition, the bacterial inoculum was taken from a 24 h-old culture, adjusted to a concentration of $10^6$ CFU $mL^{-1}$, and spread on Müller–Hinton agar plates using a sterile cotton swab. An agar plate or cylinder was aseptically punched using a sterile cork borer. Freshly prepared solutions of **1** and bpy at desired concentrations (25 μL) were added into the well. The agar plates were then incubated at 37 °C for 24 h. A plate with ampicillin (10 μg per disc) was used as the control. The diameter of the inhibition zone (mm) was measured after incubation. Experiments were repeated in triplicate, and the average values were considered.

## Results and discussion

### Characterization of 2 and 3

Products **2** and **3** were characterized *via* Job's method, FT-IR spectroscopy, and ESI-MS. Job's method revealed the metal : ligand ratio (1 : $L^1$ and 1 : $L^2$) in **2** and **3** to be 1 : 2 (Fig. 2). Fig. 3(a)–(c) show the FT-IR spectra of **1**, **2**, and **3**. The spectrum of **1** exhibited bands at 636.79 and 601.88 $cm^{-1}$ corresponding to Zn–N stretching vibrations and 733.79 and 763.11 $cm^{-1}$ corresponding to Zn–O stretching vibrations.[35] The IR spectrum of **2** showed bands at 612.25 and 582.50 $cm^{-1}$ corresponding to Zn–N bonds and 412.77 $cm^{-1}$ corresponding to the newly formed Zn–S bonds in **2**. The IR spectrum of **3** exhibited a band at ~416.77 $cm^{-1}$ corresponding to the newly formed Zn–S bond and 601.79 $cm^{-1}$ corresponding to the Zn–N bonds.[35,36]

Fig. 4(a)–(c) show the ESI-MS spectra of **1**, **2**, and **3**. The signals at 187.97, 279.93, 434.99, and 618.88 (Fig. 4(a)) correspond to [$Zn^{2+}$ + 2bpy], [$Zn^{2+}$ + 2bpy + $OAc^-$ + $HClO_4$ + $Na^+$], [$Zn^{2+}$ + 2bpy + $OAc^-$], and [$Zn^{2+}$ + 2bpy + 2$OAc^-$ + $HClO_4$ + $Na^+$], respectively. The signals at 264.995 and 188.05 (Fig. 4(b)) are attributed to [$Zn^{2+}$ + 2bpy + 2D-penicillamine + $H_2O$ + $ClO_4^-$ + $2H^+$] and [$Zn^{2+}$ + 2bpy], respectively. The signals at 254.95 and 188.03 (Fig. 4(c)) correspond to [$Zn^{2+}$ + 2bpy + 2L-cysteine + $H_2O$ + $ClO_4^-$ + $Na^+$] and [$Zn^{2+}$ + 2bpy], respectively.

### Kinetic studies

The p$K_a$ values for $L^1$ are 1.90 (COOH), 7.88 (SH), and 10.58 ($NH_2$) (Scheme 1),[37] and those for $L^2$ are 1.71 (COOH), 8.53 (SH), and 10.36 ($NH_2$) (Scheme 2).[38,39] These p$K_a$ values suggest that the S-containing ligands participate in the reactions in their anionic form (thiolate) at pH 7.4.

The plot of $\ln(A_t - A_\infty)$ *vs.* $t$ was non-linear; $A_t$ and $A_\infty$ are absorbances at time $t$ and after completion of the reaction, respectively (Fig. 5(a)). The plot curved initially before appearing linear with a constant slope. This indicates that the interactions of $L^1$ and $L^2$ with **1** proceed through two distinct steps (curved

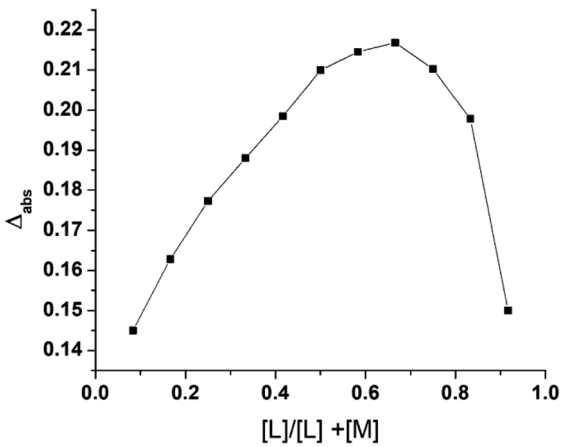


Fig. 2 Job's plot for the $L^2$-substituted product **3**.

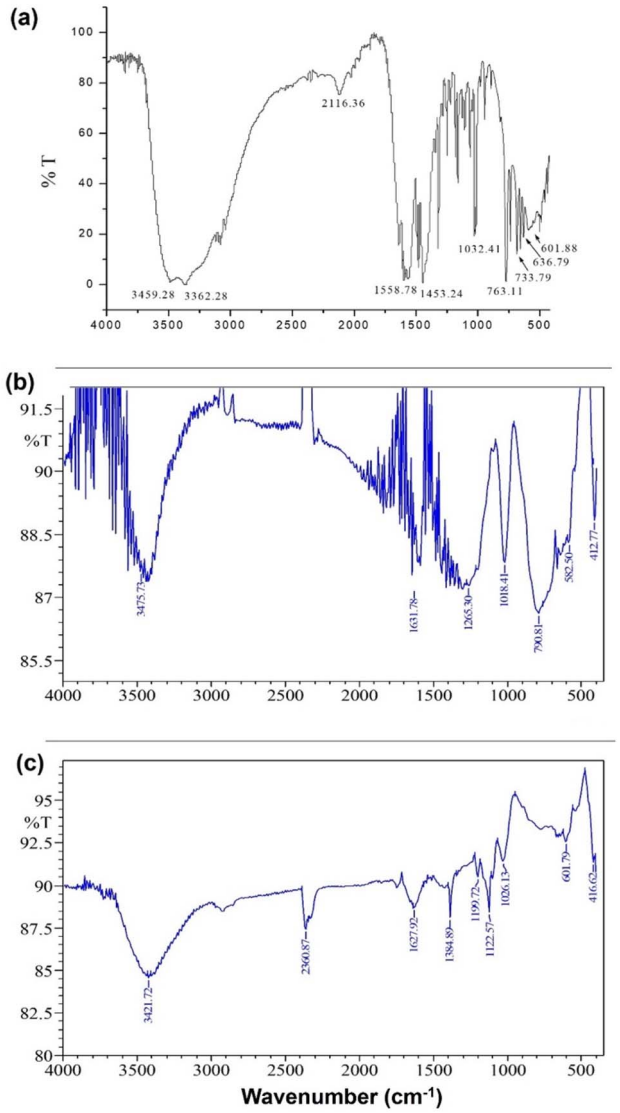


Fig. 3 FT-IR spectra of (a) **1**, (b) $L^1$-substituted product **2**, and (c) $L^2$-substituted product **3**.

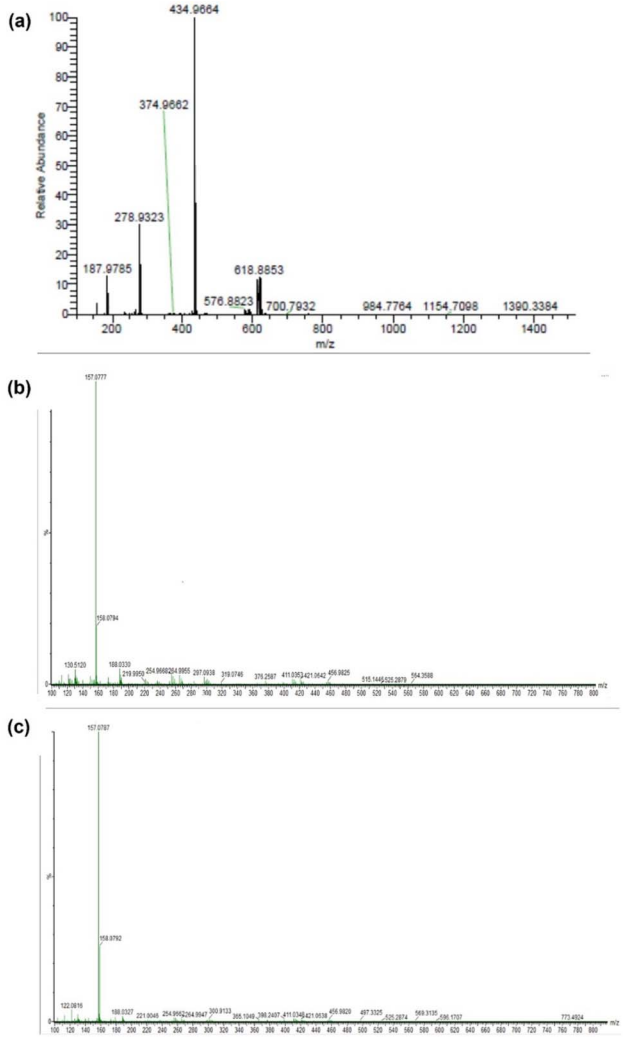


Fig. 4 ESI-MS spectrum of (a) **1**, (b) $L^1$-substituted product **2**, and (c) $L^2$-substituted product **3**.

and linear). Scheme 3 was used to calculate the rate constants for both steps.

**Calculation of $k_1$ of step A → B.** Weyh and Hamm's method[40] was employed to calculate $k_{1(obs)}$ values from the typical plots of ln $\Delta$ *vs.* $t$ without using Origin software, as the slope of the best-fitted line of the first part of the $\ln(A_\infty - A_t)$ *vs.* $t$ plot did not work for calculations shown in Fig. 5(a).

$$(A_t - A_\infty) - a_2 \exp(-k_2 t) = a_1 \exp(-k_{1(obs)} t) \quad (5)$$

where $a_1$ and $a_2$ are constants. The values of $[(A_t - A_\infty) - a_2 \exp(-k_2 t)]$ were calculated from $X$–$Y$ values at different time intervals (Fig. 6(a)) and denoted as the '$\Delta$' values.

Then, eqn (5) becomes

$$\ln \Delta = \text{constant} - k_{1(obs)} t \quad (6)$$

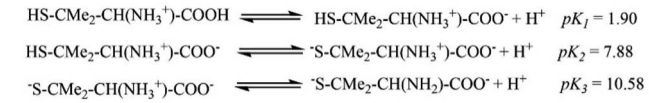


Scheme 1 The p$K_a$ values for $L^1$.

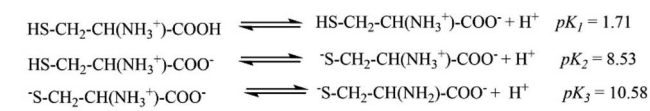


Scheme 2 The p$K_a$ values for and $L^2$.

The $k_{1(obs)}$ was calculated from the slopes of ln $\Delta$ *vs.* $t$ plots (Fig. 5(b)) at ligand concentrations of 2.0, 3.0, and 4.0 × $10^{-3}$ mol $L^{-1}$ at fixed [**1**], pH 7.4, ionic strength of 0.1 mol $L^{-1}$ $NaClO_4$, and different temperatures (20, 25, 30, and 35 °C). Tables 1 and 2 present the $k_{1(obs)}$ data.

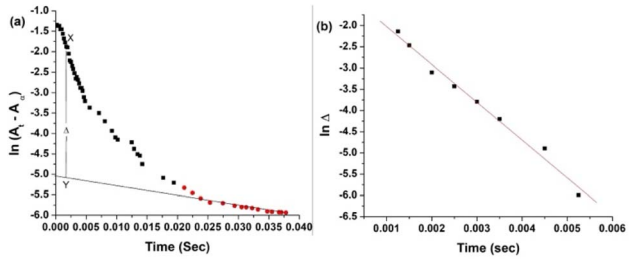


Fig. 5 (a) $\ln(A_t - A_\infty)$ *vs.* $t$ and (b) $\ln \Delta$ *vs.* $t$ plots. [**1**] $= 2 \times 10^{-4}$ mol L$^{-1}$, [ligand] $= 4 \times 10^{-3}$ mol L$^{-1}$, pH $= 7.4$, and temperature $= 35 \pm 0.1$ °C. $X-Y$ = the difference between the absorbances of the two steps in the time interval.

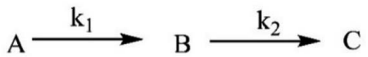


Scheme 3 Interaction of complex **1** with $L^1$ and $L^2$ and product formation, where A, B, and C represent **1**, intermediate product, and substituted product, respectively, and $k_1$ and $k_2$ are the rate constants for the first and second steps, respectively.

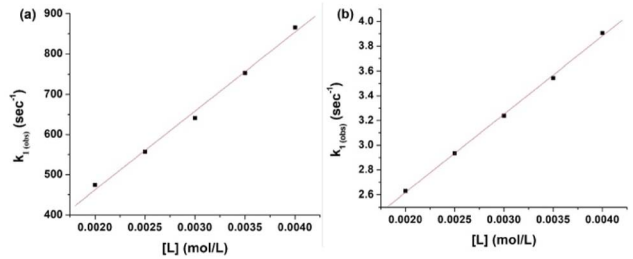


Fig. 6 $k_{1(obs)}$ *vs.* (a) [$L^1$] and (b) [$L^2$] at a fixed pH (7.4) and temperature (25 ± 0.1 °C).

The plots of $k_{1(obs)}$ *vs.* [L] (Fig. 6(a) and (b)) are straight lines. The $k_1$ values (slopes of the plots) at different [L] and temperatures (Tables 3 and 4) demonstrate that the rate increased as the [L] increased. The first step was ligand-dependent, which indicates that $L^1$ or $L^2$ attacks Zn(II) to form intermediate B in this step (Scheme 3).

**Calculation of $k_2$ for step B → C.** The $k_{2(obs)}$ values were calculated from the linear segment of $\ln(A_t - A_\infty)$ *vs.* $t$ plot (Fig. 5(a) and Table 5). The plots of $k_{2(obs)}$ *vs.* [L] were also straight lines (Fig. 7(a) and (b)). The $k_{2(obs)}$ values increased with increasing [L] (Fig. 7 and Table 5). The $k_2$ values (Table 6), which are the slopes of the plots at four temperatures (Fig. 7(a) and (b)), increased with increasing [L]. Therefore, the second step is ligand-dependent.

Table 1 $10^{-2}$ $k_{1(obs)}$ values (s$^{-1}$) for $L^1$ at five different concentrations, four different temperatures, and constant pH (7.4), ionic strength (0.1 mol per L $NaClO_4$), and [**1**] ($2 \times 10^{-4}$ mol L$^{-1}$)

| | | $10^3$ [ligand] mol L$^{-1}$ | | | | |
|---|---|---|---|---|---|---|
| | System temperature (°C) | 2.0 | 2.5 | 3.0 | 3.5 | 4.0 |
| $L^1$ | 20 | 4.54 | 5.27 | 5.95 | 6.72 | 7.50 |
| | 25 | 4.73 | 5.57 | 6.40 | 7.53 | 8.65 |
| | 30 | 4.78 | 5.72 | 6.66 | 7.83 | 9.01 |
| | 35 | 5.00 | 6.05 | 7.12 | 8.37 | 9.63 |

Table 2 $10^{-2}$ $k_{1(obs)}$ values (s$^{-1}$) for $L^2$ at five different concentrations, four different temperatures, and constant pH (7.4), ionic strength (0.1 mol per L $NaClO_4$), and [**1**] ($2 \times 10^{-4}$ mol L$^{-1}$)

| | | $10^3$ [ligand] mol L$^{-1}$ | | | | |
|---|---|---|---|---|---|---|
| | System temperature (°C) | 2.0 | 2.5 | 3.0 | 3.5 | 4.0 |
| $L^2$ | 20 | 1.51 | 2.13 | 2.75 | 3.39 | 3.83 |
| | 25 | 2.63 | 2.94 | 3.24 | 3.65 | 4.05 |
| | 30 | 2.71 | 3.71 | 4.72 | 6.32 | 7.91 |
| | 35 | 5.06 | 7.03 | 9.00 | 10.4 | 11.8 |

**Effect of temperature on $k_1$ and $k_2$.** Both $k_1$ (Tables 3 and 4) and $k_2$ (Table 6) increased with increasing operating temperatures. This suggests that the two substitution reactions are highly temperature-sensitive. Hence, their activation and thermodynamic parameters were evaluated using the Eyring equation. The Eyring plots ($\ln k_r h/k_B T$ *vs.* $1/T$) for the first and second steps of the reaction of $L^1$ and **1** are shown in Fig. 8(a) and (b), whereas those of $L^2$ are shown in Fig. 8(c) and (d). The enthalpy of activation values ($\Delta H_1^{\neq}$ and $\Delta H_2^{\neq}$) and the entropy of activation values ($\Delta S_1^{\neq}$ and $\Delta S_2^{\neq}$) are obtained from the slopes and the intercepts of the Eyring plots, respectively. The activation and thermodynamic parameters are listed in Table 7. The positive enthalpy and negative entropy values (Table 7) confirm the ligand dependency of **1** and the ligand interactions at each step.

**Mechanism.** The p$K_a$ values of $L^1$ and $L^2$ at 25 °C suggest that the S-containing ligands exist in their thiolate forms at pH 7.4. Job's method and FT-IR and ESI-MS spectra of **1**, **2**, and **3** confirm that $L^1$ and $L^2$ act as monodentate ligands, binding their S atoms to Zn, considering the predominant existence of ZnS in zinc ores.[41]

The highly negative $S_1^{\neq}$ and $\Delta S_2^{\neq}$ and the less positive $\Delta H_1^{\neq}$ and $\Delta H_2^{\neq}$, determined from $\ln(A_t - A_\infty)$ *vs.* $t$ plots (Fig. 5(a)), indicate an associative mode of activation with two distinct steps (Scheme 3). Moreover, the rate constants ($k_1$ and $k_2$) depended on the ligand concentration. This suggests that, in the first step, one molecule of L attacks the Zn(II) to form intermediate B, which is further attacked by a second molecule of L to form the product.

The energy required for Zn–OAc bond cleavage is compensated by the energy released during Zn–L bond formation. The

Table 3 $k_1$ values of $L^1$ at four different temperatures and constant pH (7.4), ionic strength (0.1 mol per L $NaClO_4$), and [**1**] ($2 \times 10^{-4}$ mol L$^{-1}$)

| Ligand | Temperature (°C) | $10^{-5}$ $k_1$ (L mol$^{-1}$ s$^{-1}$) |
|---|---|---|
| $L^1$ | 20 | 1.48 ± 0.02 |
| | 25 | 1.96 ± 0.08 |
| | 30 | 2.15 ± 0.07 |
| | 35 | 2.31 ± 0.06 |

Table 4 $k_1$ values of $L^2$ at four different temperatures and constant pH (7.4), ionic strength (0.1 mol per L $NaClO_4$), and [**1**] ($2 \times 10^{-4}$ mol $L^{-1}$)

| Ligand | Temperature (°C) | $10^{-1}$ $k_1$ (L $mol^{-1}$ $s^{-1}$) |
|---|---|---|
| $L^2$ | 20 | 1.27 ± 0.017 |
| | 25 | 1.67 ± 0.05 |
| | 30 | 2.56 ± 0.31 |
| | 35 | 3.36 ± 0.32 |

Table 5 $10^{-2}$ $k_{2(obs)}$ values ($s^{-1}$) of $L^1$ and $L^2$ at four different temperatures and three different concentrations and constant pH (7.4), ionic strength (0.1 mol per L $NaClO_4$), and [**1**] ($2 \times 10^{-4}$ mol $L^{-1}$)

| | System temperature (°C) | $10^3$ [ligand] mol $L^{-1}$ | | | | |
|---|---|---|---|---|---|---|
| | | 2.0 | 2.5 | 3.0 | 3.5 | 4.0 |
| $L^1$ | 20 | 2.51 | 5.15 | 6.62 | 10.25 | 12.73 |
| | 25 | 3.07 | 6.17 | 8.57 | 12.79 | 17.01 |
| | 30 | 3.75 | 8.13 | 12.50 | 15.95 | 21.11 |
| | 35 | 5.01 | 9.80 | 14.50 | 18.75 | 23.01 |
| $L^2$ | 20 | 4.35 | 6.55 | 8.85 | 11.71 | 14.55 |
| | 25 | 5.00 | 7.45 | 10.10 | 13.35 | 16.64 |
| | 30 | 6.67 | 9.88 | 13.10 | 16.66 | 20.22 |
| | 35 | 7.40 | 10.90 | 14.50 | 18.05 | 22.50 |

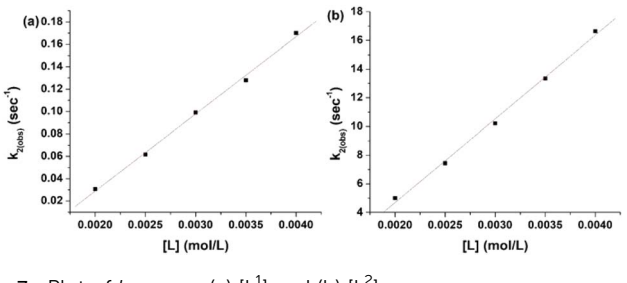


Fig. 7 Plot of $k_{2(obs)}$ *vs.* (a) [$L^1$] and (b) [$L^2$].

Table 6 $10^{-1}$ $k_2$ values of $L^1$ and $L^2$ at four temperatures and constant pH (7.4), ionic strength (0.1 mol per L $NaClO_4$), and [**1**] ($2 \times 10^{-4}$ mol $L^{-1}$)

| Ligand | Temperature (°C) | $10^{-1}$ $k_2$ (L $mol^{-1}$ $s^{-1}$) |
|---|---|---|
| $L^1$ | 20 | 5.10 ± 0.11 |
| | 25 | 6.96 ± 0.70 |
| | 30 | 8.67 ± 0.04 |
| | 35 | 9.00 ± 0.007 |
| $L^2$ | 20 | 5.07 ± 0.33 |
| | 25 | 5.85 ± 0.43 |
| | 30 | 6.66 ± 0.13 |
| | 35 | 7.55 ± 0.25 |

low $\Delta H_1^{\neq}$ and $\Delta H_2^{\neq}$ values support this inference. Our proposed mechanism is shown in Fig. 9.

## Bioassays

**Electronic absorption titration.** A metal complex can bind to the DNA double helix through intercalation[42] or non-interactive

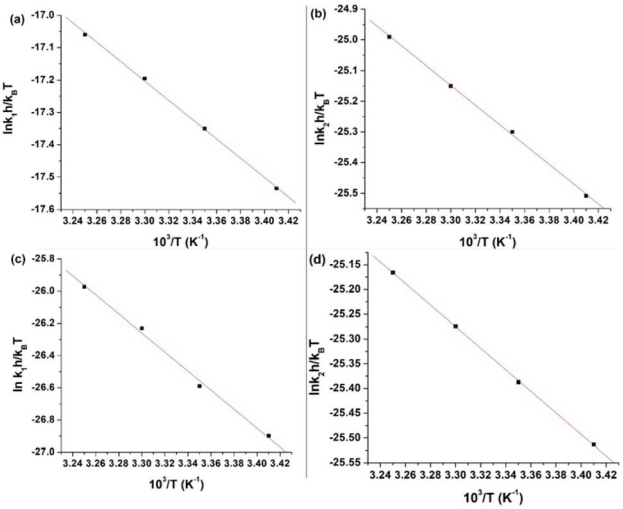


Fig. 8 Eyring plots (a) $\ln k_1h/k_BT$ *vs.* $10^3/T$ for the A → B step of $L^1$, (b) $\ln k_2h/k_BT$ *vs.* $10^3/T$ for the B → C step of $L^1$, (c) $\ln k_1h/k_BT$ *vs.* $10^3/T$ for the A → B step of $L^2$, and (d) $k_2h/k_BT$ *vs.* $10^3/T$ for the B → C step of $L^2$.

modes, such as covalent, ionic, hydrophobic, and hydrogen bonds, as well as van der Waals interactions. The mode of interaction is reflected by (i) a change in absorption intensity (hyper or hypochromism) and (ii) a red or blue shift of the band.[43]

Fig. 10 shows the electronic absorption titration spectra of different ctDNA concentrations at a constant [**1**]. The absorption intensity decreased with increasing ctDNA concentrations without a red or blue shift (Fig. 10(a)). This hypochromism indicates an intercalative binding mode between **1** and ctDNA.[44,45] The plot of [DNA]/($\varepsilon_b - \varepsilon_f$) *vs.* [DNA] is linear (Fig. 10(b)). The $K_b$ value (binding constant, $2.5 \times 10^4$ $M^{-1}$) obtained from the slope of the plot indicates moderate to strong binding between **1** and ctDNA.

**Fluorescence emission titration.** An aqueous solution of **1** at room temperature and working pH did not fluoresce with or without DNA. The fluorescence intensity was too low for a solution of EtBr in Tris–HCl buffer (pH 7.4) in the absence of DNA. In contrast, the fluorescence intensity increased ~20-fold in the presence of ctDNA, which suggests strong intercalation with the dye (EtBr).[45,46] Therefore, a fluorescence quenching titration was performed to determine the binding nature of **1** and DNA.

Increasing the concentration of **1** decreased the emission intensity of the EtBr–DNA solution owing to successive quenching. This indicates competition between **1** and EtBr for ctDNA binding (Fig. 11(a)). The $K_{sv}$ value of $1.5 \times 10^3$ $M^{-1}$ was obtained using the Stern–Volmer plot, whereas $K_F$ ($4.57 \times 10^6$ $M^{-1}$) and $n$ (1.4) values were obtained using Scatchard plots of **1** and ctDNA (Fig. 11(b) and (c)).

**Agarose gel electrophoresis.** The nuclease activity of **1** was investigated using plasmid DNA (pBR322). The efficiency of the Zn(II) complex in transforming the original form of DNA (closed circular supercoiled; form I) into a relaxed or nicked form (form II) or a linear form (form III) was evaluated.[30] Complex **1**

Table 7 Activation and thermodynamic parameters for the reaction

| Ligand | $\Delta H_1^{\neq}$ (kJ mol$^{-1}$) | $\Delta S_1^{\neq}$ (J K$^{-1}$ mol$^{-1}$) | $\Delta H_2^{\neq}$ (kJ mol$^{-1}$) | $\Delta S_2^{\neq}$ (J K$^{-1}$ mol$^{-1}$) |
|---|---|---|---|---|
| $L^1$ | 24.81 ± 0.54 | −61 ± 1 | 26.76 ± 0.55 | −120 ± 1 |
| $L^2$ | 49.51 ± 2.33 | −56 ± 2 | 18.09 ± 0.16 | −150 ± 0.5 |

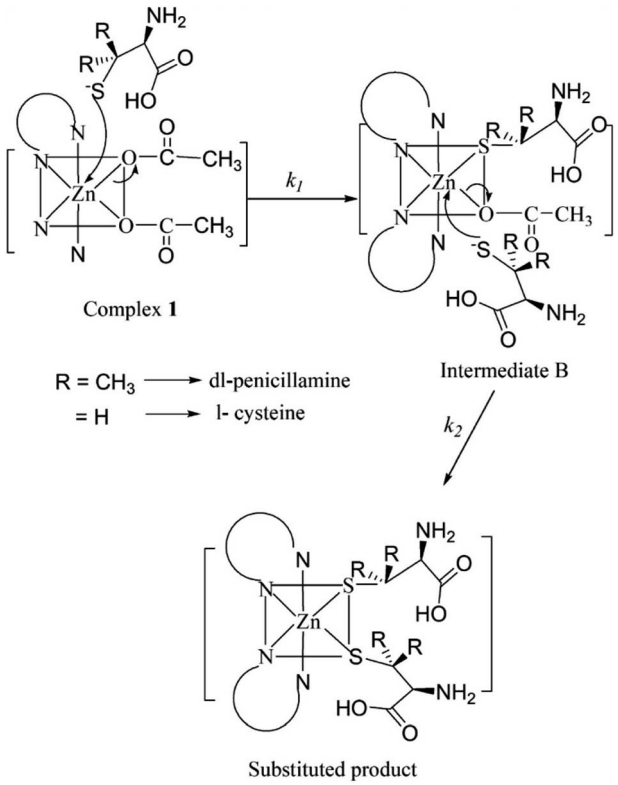


Fig. 9 Plausible mechanism of the substitution reactions of **1** and $L_1$/$L_2$.

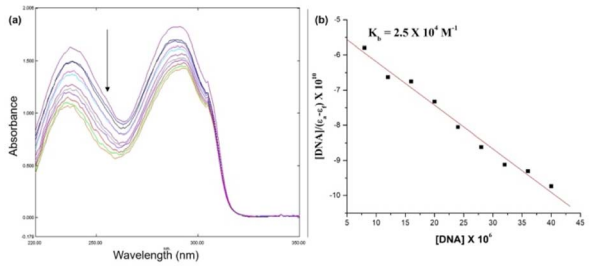


Fig. 10 (a) Electronic absorption spectra were obtained during the titration of 0.1 mM of **1** in Tris–HCl buffer with different [ctDNA] (0–20 μM). The arrow indicates a decrease in intensity upon the addition of ctDNA. (b) Linear fit of [DNA]/($\varepsilon_a - \varepsilon_f$) *vs.* [DNA].

successfully cleaved plasmid DNA into different sizes in the absence of any precursors (*e.g.*, UV light or reducing agent) at all concentrations (29, 50, 67, and 80 μM) (Fig. 12; lanes 1 to 4; untreated plasmid DNA was the control). All three forms of DNA were observed after digestion with **1**. Moreover, DNA mobility from form-I to forms-II and III decreased, and the rate of digestion of plasmid DNA increased with increasing [**1**].[47] Moreover, fainter bands (lanes 2–4) appeared at higher [**1**], confirming DNA degradation. Hence, the extent of DNA

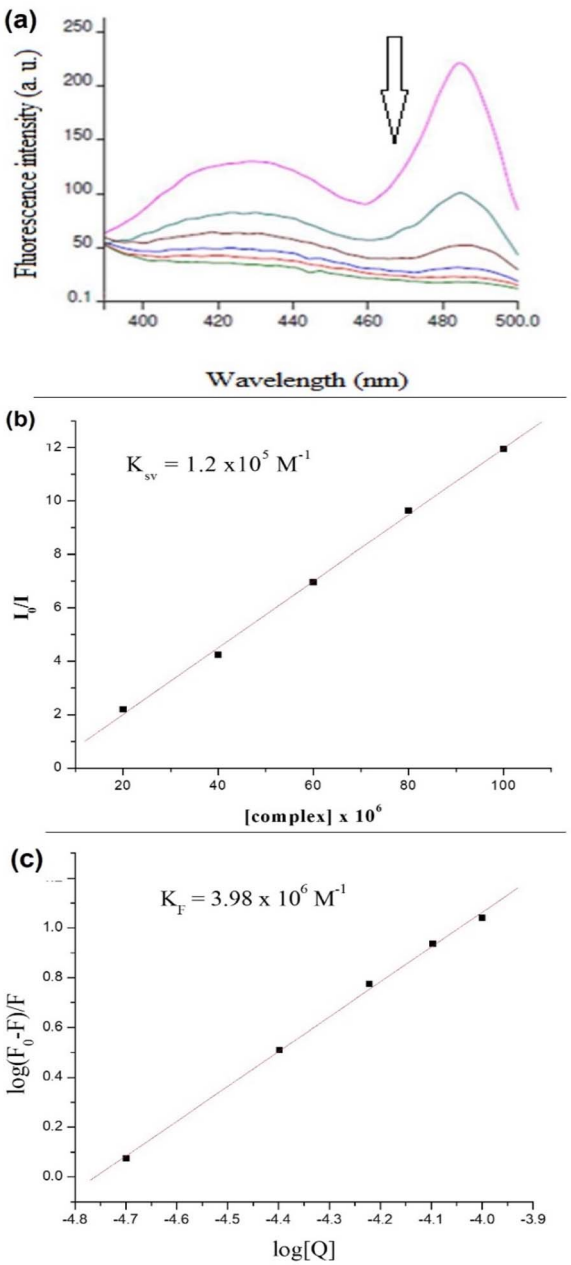


Fig. 11 (a) Fluorescence spectra at increasing [**1**] (10–100 μM) in an EtBr–DNA solution of pH 7.4 (Tris–HCl buffer); (b) Stern–Volmer plot and determination of $K_{sv}$; and (c) Scatchard plot of **1** and ctDNA and determination of $K_F$ and *n*.

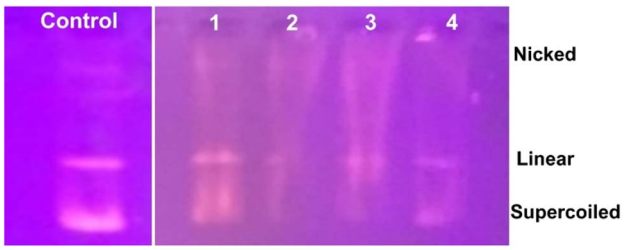


Fig. 12 Gel electrophoresis of plasmid DNA treated with **1**.

digestion is directly proportional to the initial [**1**]. The smear observed in the four lanes is attributed to EtBr, which strongly interacts with the complex.[30]

**Antimicrobial assay.** The antimicrobial activity of **1** against fungal and bacterial strains was evaluated. The results of agar well diffusion are summarized in Table 8. A clear zone around the well (Fig. 13) confirmed that **1** inhibited the growth of Gram-positive and Gram-negative bacterial strains. This illustrates the bioactivity of a Zn(II)–bpy complex.[48] The activity increased with increasing [**1**]. In particular, **1** was more effective against Gram-positive bacteria (Fig. 13). This may be due to the different cell wall structures of Gram-positive and Gram-negative bacteria. Complex **1** was ineffective against *Aspergillus niger* and Gram-negative *Enterobacter asburiae* but was effective against *Escherichia coli*. In addition, lower to higher concentrations of bpy were effective against *E. coli* but not against *S. aureus*. Hence, this complex can be a new, cost-effective antimicrobial agent to combat microbes which are resistant to conventional antimicrobials. Sinha *et al.* reported that 2–10 mM ZnO significantly inhibited the growth of Gram-negative bacteria (*Enterobacter* sp.) but showed a minimal effect on Gram-positive bacteria (*Bacillus subtilis*), with an insignificant reduction in the viable bacterial count.[49]

We propose a mechanism for the antimicrobial activity of **1** based on the literature and our findings (Fig. 14).[50] The charge

Table 8 Diameters of the inhibition zones (bearing a spectator ligand) of selected microbes at increasing [**1**][a]

| | Zone of inhibition (mm) | | | | | | | |
|---|---|---|---|---|---|---|---|---|
| Microorganisms | bpy | L | $M_1$ | $M_2$ | H | $H_1$ | $H_2$ | $H_3$ |
| **Gram-negative bacteria** | | | | | | | | |
| *Enterobacter asburiae* | — | — | — | — | — | — | — | — |
| *Escherichia coli* | 10 | 11 | 12 | 12 | 13 | 14 | 14 | 15 |
| **Gram-positive bacteria** | | | | | | | | |
| *Staphylococcus aureus* | — | 11 | 11 | 11 | 12 | 12 | 13 | 15 |
| *Bacillus subtilis* | <10 | 11 | 11 | 11 | 12 | 13 | 14 | 15 |
| *Salinicoccus roseus* | 11 | 12 | 13 | 13 | 14 | 14 | 15 | 16 |
| *Halomonas denitrificans* | 11 | 12 | 12 | 13 | 14 | 15 | 15 | 15 |
| **Fungus** | | | | | | | | |
| *Aspergillus niger* | — | — | — | — | — | — | — | — |

[a] $[L] = 0.5 \times 10^{-3}$ M; $[M_1] = 1.0 \times 10^{-3}$ M; $[M_2] = 1.5 \times 10^{-3}$ M; $[H] = 2.0 \times 10^{-3}$ M; $[H_1] = 2.5 \times 10^{-3}$ M; $[H_2] = 3.0 \times 10^{-3}$ M; and $[H_3] = 3.5 \times 10^{-3}$ M.

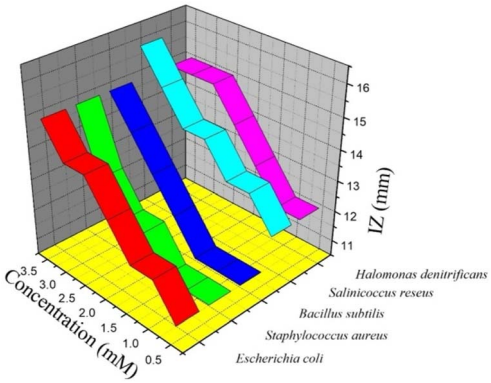


Fig. 13 Effect of **1** on microbial growth estimated by inhibition zone (IZ).

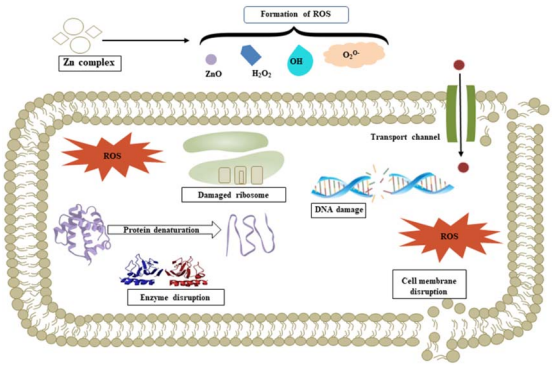


Fig. 14 Plausible antimicrobial mechanism of **1**.

density of $Zn^{2+}$ is reduced to chelation in **1**, which reduces its hydrophilicity and enhances lipophilicity. This enables its quick entry through the cell membrane (due to its lipidic nature).[51,52] Then, **1** participates in bactericidal (killing) or bacteriostatic (blocking of active sites) mechanisms. An increase in $Zn^{2+}$ concentration above the optimal limit disrupts ion homeostasis. This allows the efflux of $Zn^{2+}$ inside the cell, causing a cytotoxic effect. Moreover, $Zn^{2+}$ has been attributed to the upregulation of ROS, which leads to oxidative stress in bacterial cells. This is consistent with previous reports, which demonstrated that the antimicrobial properties of Zn-based complexes are correlated to ROS overproduction, which may be the underlying mechanism for cell death caused by DNA damage.[50,53] The increased membrane permeability of bacterial cells, mediated by $Zn^{2+}$, facilitates ion channel dysfunction. This disrupts respiratory processes and reduces energy-producing adenosine triphosphate synthesis.

## Conclusions

A novel six-coordinate Zn(II) complex was synthesized and characterized using electronic, FT-IR, and ESI-MS spectroscopy. Kinetic and mechanistic investigations were performed in an aqueous medium and under pseudo-first-order reaction conditions at physiological pH with two bio-relevant ligands

bearing N, O, and S donor atoms. These substitution reactions involved two distinct ligand-dependent steps. Highly negative entropy of activation values and less positive enthalpy of activation values suggested an associative activation mode. The rate constants ($k_1$) were in the following order: $L^1$ (DL-penicillamine) $\gg$ $L^2$ (L-cysteine). This was attributed to the lower p$K_2$ value (SH) and +I effect of two methyl groups at the $C_\beta$ of $L^1$. Even though both ligands have S and N donor sets, the ligands were bonded to Zn(II) *via* their S end. *In vitro*, DNA-binding studies indicated a positive interaction between **1** ($[Zn(bpy)_2(OAc)_2]$) and ctDNA. We also demonstrated the bactericidal and fungicidal effects of **1** against selected microbial strains. This study can be summarized as follows: (i) selection of a non-toxic metal center (Zn(II)); (ii) kinetic investigation to elucidate the selectivity and reactivity of different ligands; (iii) elucidation of DNA binding and cleavage capacity; and (iv) exploration of the antimicrobial activity of **1**.

## Data availability

Data supporting this study are openly available from Prof. Alak K. Ghosh.

## Conflicts of interest

There are no conflicts to declare.

## Acknowledgements

This work was supported by the National Research Foundation of Korea (NRF) grant funded by the Korean Government (MSIT) (No. RS-2023-00219983). Moonis Ali Khan acknowledges financial support through the Researchers Supporting Project (RSP2024R345), King Saud University, Riyadh, Saudi Arabia. Another author (Dr R. Kumar) acknowledges support from the Creative and Challenging Research Program [grant number 2021R1I1A1A01060846] of the National Research Foundation (NRF) of the Republic of Korea.

## References

1 S. Abdolmaleki, A. Aliabadi and S. Khaksar, *Coord. Chem. Rev.*, 2024, **501**, 215579.
2 S. Adhikari, P. Nath, A. Das, A. Datta, N. Baildya, A. K. Duttaroy and S. Pathak, *Biomed. Pharmacother.*, 2024, **171**, 116211.
3 M. Porchia, M. Pellei, F. Del Bello and C. Santini, *Molecules*, 2020, **25**, 5814.
4 R. Ye, C. Tan, B. Chen, R. Li and Z. Mao, *Front. Chem.*, 2020, **8**, 402.
5 T. V. Soldatović, B. Šmit, E. M. Mrkalić, S. L. Matić, R. M. Jelić, M. Ć. Serafinović, N. Gligorijević, M. Čavić, S. Aranđelović and S. Grgurić-Šipka, *J. Inorg. Biochem.*, 2023, **240**, 112100.
6 S. Singh and K. Pal, *Int. J. Biol. Macromol.*, 2023, **234**, 123602.
7 S. Bhattacharyya, A. Sarkar, S. K. Dey and A. Mukherjee, *J. Inorg. Biochem.*, 2014, **140**, 131–142.
8 Z. Wang, S. Gai, C. Wang, G. Yang, C. Zhong, Y. Dai, F. He, D. Yang and P. Yang, *Chem. Eng. J.*, 2019, **361**, 117–128.
9 M. Fakhar-e-Alam, I. Amjad, M. Saadullah, M. Tahir, M. Jawad, M. Asif, M. Atif, S. Zara and M. Rashad, *J. Saudi Chem. Soc.*, 2024, **28**, 101814.
10 R. G. Pearson, *J. Am. Chem. Soc.*, 1963, **85**, 3533–3539.
11 P. Gać, K. Czerwińska, P. Macek, A. Jaremków, G. Mazur, K. Pawlas and R. Poręba, *Environ. Toxicol. Pharmacol.*, 2021, **82**, 103553.
12 C. B. Devi, T. Nandakishore, N. Sangeeta, G. Basar, N. O. Devi, S. Jamir and M. A. Singh, *IOSR J. Dent. Med. Sci.*, 2014, **13**, 18–23.
13 P. J. Fraker, L. E. King, T. Laakko and T. L. Vollmer, *J. Nutr.*, 2000, **130**, 1399S–1406S.
14 C. T. Chasapis, A. C. Loutsidou, C. A. Spiliopoulou and M. E. Stefanidou, *Arch. Toxicol.*, 2012, **86**, 521–534.
15 A. B. Lansdown, U. Mirastschijski, N. Stubbs, E. Scanlon and M. S. Ågren, *Wound Repair Regen.*, 2007, **15**, 2–16.
16 S. S. Singh, B. Jena, S. Roy, S. Nayak, S. K. Behera, S. Chakrabortty, S. K. Tripathy, M. Ali Khan, R. Kumar, B.-H. Jeon, C. Stålsby Lundborg and A. Mishra, *Chem. Eng. J.*, 2024, **490**, 151788.
17 R. S. MacDonald, *J. Nutr.*, 2000, **130**, 1500S–1508S.
18 K. Sardana and V. K. Garg, *Dermatol. Ther.*, 2010, **23**, 411–418.
19 J. Qian, L. Wang, W. Gu, X. Liu, J. Tian and S. Yan, *Dalton Trans.*, 2011, **40**, 5617–5624.
20 S. Q. Zhang, X. F. Yu, H. B. Zhang, N. Peng, Z. X. Chen, Q. Cheng, X. L. Zhang, S. H. Cheng and Y. Zhang, *Mol. Nutr. Food Res.*, 2018, **62**, e1700981.
21 M. Pellei, F. Del Bello, M. Porchia and C. Santini, *Coord. Chem. Rev.*, 2021, **445**, 214088.
22 L. P. Roguin, N. Chiarante, M. C. García Vior and J. Marino, *Int. J. Biochem. Cell Biol.*, 2019, **114**, 105575.
23 A. A. Franich, M. D. Živković, J. Milovanović, D. Arsenijević, A. Arsenijević, M. Milovanović, M. I. Djuran and S. Rajković, *J. Inorg. Biochem.*, 2020, **210**, 111158.
24 C. Y. Huang, in *Methods in Enzymology*, ed. D. L. Purich, Academic Press, 1982, vol. 87, pp. 509–525.
25 J. P. M. João, *Ann. Chim. Appl.*, 1928, 113–203.
26 E. Gao, L. Liu, M. Zhu, Y. Huang, F. Guan, X. Gao, M. Zhang, L. Wang, W. Zhang and Y. Sun, *Inorg. Chem.*, 2011, **50**, 4732–4741.
27 A. Pal, B. Biswas, S. K. Mondal, C.-H. Lin and R. Ghosh, *Polyhedron*, 2012, **31**, 671–675.
28 C. D. Kanakis, P. A. Tarantilis, M. Polissiou, S. Diamantoglou and H. Tajmir-Riahi, *Cell Biochem. Biophys.*, 2007, **49**, 29–36.
29 A. A. El-Bindary, N. Hassan and M. A. El-Afify, *J. Mol. Liq.*, 2017, **242**, 213–228.
30 I. Mitra, S. Mukherjee, V. P. Reddy B, S. Dasgupta, J. C. Bose K, S. Mukherjee, W. Linert and S. C. Moi, *RSC Adv.*, 2016, **6**, 76600–76613.
31 P. Borst, *IUBMB Life*, 2005, **57**, 745–747.
32 M. Balouiri, M. Sadiki and S. K. Ibnsouda, *J. Pharm. Anal.*, 2016, **6**, 71–79.
33 R. Geetha, C. Sathian, V. Prasad and V. Gleeja, *Asian J. Dairy Food Res.*, 2015, **34**, 259–264.

34 P. Ristivojević, I. Dimkić, J. Trifković, T. Berić, I. Vovk, D. Milojković-Opsenica and S. Stanković, *PLoS One*, 2016, **11**, e0157097.
35 D. Huang, Q. Xin, Y. Ni, Y. Shuai, S. Wang, Y. Li, H. Ye, L. Lin, X. Ding and Y. Zhang, *RSC Adv.*, 2018, **8**, 6099–6109.
36 L.-N. Liu, J.-G. Dai, T.-J. Zhao, S.-Y. Guo, D.-S. Hou, P. Zhang, J. Shang, S. Wang and S. Han, *RSC Adv.*, 2017, **7**, 35075–35085.
37 A. E. Martell and R. M. Smith, *Critical Stability Constants*, Springer, 1974.
38 G. Hager and A. G. Brolo, *J. Electroanal. Chem.*, 2009, **625**, 109–116.
39 A. H. Dourado, A. P. de Lima Batista, A. G. Oliveira-Filho, P. T. Sumodjo and S. I. C. de Torresi, *RSC Adv.*, 2017, **7**, 7492–7501.
40 J. A. Weyh and R. E. Hamm, *Inorg. Chem.*, 1969, **8**, 2298–2302.
41 F. A. Cotton, G. Wilkinson, C. A. Murillo and M. Bochmann, *Advances in Inorganic Chemistry*, John Wiley & Sons, 1999.
42 B. M. Zeglis, V. C. Pierre and J. K. Barton, *Chem. Commun.*, 2007, 4565–4579, DOI: **10.1039/B710949K**.
43 F. Arjmand, M. Aziz and M. Chauhan, *J. Inclusion Phenom. Macrocyclic Chem.*, 2008, **61**, 265–278.
44 M. J. Brabha and M. A. Malbi, *Chem. Phys. Impact*, 2023, **7**, 100248.
45 F. Arjmand and M. B. Chauhan, *Helv. Chim. Acta*, 2005, **88**, 2413–2423.
46 C.-L. Zhang, D.-H. Cai, S. Chen, W. Liu, Y.-H. Xiong and X.-Y. Le, *Transition Met. Chem.*, 2019, **44**, 603–613.
47 Q. Zhang, Y. Xiang, D. Liang, Y. Peng and H. Guo, *Bioorg. Med. Chem. Lett.*, 2012, **22**, 1814–1817.
48 S. P. Santoso, S. Ismadji, A. E. Angkawijaya, F. E. Soetaredjo, A. W. Go and Y. H. Ju, *J. Mol. Liq.*, 2016, **221**, 617–623.
49 R. Sinha, R. Karan, A. Sinha and S. K. Khare, *Bioresour. Technol.*, 2011, **102**, 1516–1520.
50 I. Matai, A. Sachdev, P. Dubey, S. Uday Kumar, B. Bhushan and P. Gopinath, *Colloids Surf., B*, 2014, **115**, 359–367.
51 Pranjal, G. Chandra Mahapatra, S. Chakrabortty, S. Banerjee, S. Chowdhury, M. Ali Khan, R. Kumar, B.-H. Jeon, A. Mishra, C. Stålsby Lundborg and S. K. Tripathy, *Chem. Eng. J.*, 2024, **497**, 154670.
52 B. Jena, S. S. Singh, S. Chakrabortty, S. K. Behera, S. K. Tripathy, C. S. Lundborg, R. Kumar, M. Ali Khan, B. H. Jeon and A. Mishra, *J. Ind. Eng. Chem.*, 2024, DOI: **10.1016/j.jiec.2024.04.049**.
53 F.-Y. Wang, Q.-Y. Xi, K.-B. Huang, X.-M. Tang, Z.-F. Chen, Y.-C. Liu and H. Liang, *J. Inorg. Biochem.*, 2017, **169**, 23–31.